Study of low Reynolds number hydrodynamics generated by symmetric corotating two-roll mills

Marco A.H. Reyes and Enrique Geffroy

Instituto de Investigaciones en Materiales, Universidad Nacional Autónoma de México
Cd. Universitaria, 04510 México, D.F., Mexico

A Closed-form analytical solution for the creeping flow equations in bipolar cylindrical coordinates is presented and used to study the flow generated by a corotating symmetric two-roll mill. The flow field has a stagnation point where elongational flow conditions exist. The geometric characteristics of the mill define the ratio of vorticity to rate of deformation that exists at the stagnation point. The solution is based upon Jeffery's solution of the biharmonic equation obtained for the stresses on a plate [*Proc. Roy. Soc. London A* **101** (1922) 169]. The streamlines, the velocity field, the magnitude of the velocity gradient and other properties of the flow are obtained for the complete flow domain. For the region around the stagnation point, the calculated results show good agreement with the numerical predictions of Singh and Leal [*J. Rheology* **38** (1994) 485] and the experimental measurements of Wang *et al.* [*Phys. Fluids* **6** (1994) 3519]. This solution should be useful for investigations of the dynamics of drops, elastic capsules, or studies of chaotic advection, where exact solutions are necessary benchmarks.

Keywords: Elongational flows; two-roll mills; stokes flow

Se presenta una solución analítica cerrada para el flujo de Stokes generado por un molino de dos rodillos. El flujo generado tiene un punto de estancamiento en el centro del molino en donde existen condiciones de flujo elongacional. Las características geométricas del molino determinan la razón de vorticidad entre la rapidez de deformación que existe en el punto de estancamiento. La solución se basa en la solución de Jeffery de la ecuación biharmónica obtenida para los esfuerzos sobre una placa [*Proc. Roy. Soc. London A* **101** (1922) 169]. Las líneas de corriente, el campo de velocidades, la magnitud del gradiente de velocidades y otras propiedades del dominio completo del flujo también se dan. Para la región alrededor del punto de estancamiento, los resultados calculados tienen buena concordancia con las predicciones numéricas del Singh & Leal [*J. Rheology* **38** (1994) 485] y los resultados experimentales de Wang *et al.* [*Phys. Fluids* **6** (1994) 3519]. La solución será de utilidad para investigaciones en la dinámica de gotas, cápsulas elásticas o para estudios de advección caótica, en donde las soluciones exactas son patrones de referencia indispensables.

Descriptores: Flujo elongacional; molino de dos rodillos; flujo de stokes

PACS: 47.55.Dz; 47.80.+v; 83.50.-v

1. Introduction

The two-roll mill consists of two cylinders of equal radii, with colinear axes, and separated by a small distance. The analytical solution assumes a steady, two-dimensional flow as if generated by rollers of infinite length and rotating with equal angular velocities. Inertial terms are considered negligible. For corotating two-roll mills, there exists a stagnation point on the line between the cylinders' axes, with local kinematic conditions characteristic of elongational flow with some vorticity. According to Chong *et al.* [1], the stagnation point corresponds to a two-dimensional critical point where all three velocity components are zero, and the slope of the streamline is indeterminate. Unlike many other critical points, in the case of the two-roll mill the kinematics is defined only by the angular velocity of the rollers, and by their geometric aspect, *i.e.*, the cylinders' diameter and the separation between them. When identical cylinders rotate at the same speed, the stagnation point is located at equal distances from the centers of rotation. In this case, the gap between the rollers and their radii also determine the ratio of the rate of deformation to vorticity that exists in the neighborhood around the stagna-

tion point. Hence, one of the interesting features of the elongational flow field generated by these mills is the fact that the solution takes into account, firstly, the presence of the rollers at a finite distance, and secondly, that the flow parameters are defined only by the mill's geometry.

Given that bipolar cylindrical coordinates are the natural reference frame for systems composed of two cylinders, an important set of flow devices have already been theoretically and experimentally studied. In 1922, G.B. Jeffery [2] presented a solution for the Stokes flow generated *inside the annular region of eccentric cylinders*. The solution prescribes the boundary of the cylinders by constant values of one of the bipolar coordinates [3, 4] for a stream-function that satisfies the biharmonic equation. Jeffery [2] gave also a solution for a *counter-rotating* two-roll mill in an unbounded fluid. For this flow, fluid is drawn in in one direction and driven out in the opposite direction. In 1925, R.A. Frazer [6] used Stokes' "principle of successive reflections" [4, 7] to study flows generated by two rotating cylinders in a viscous fluid. In particular, a solution is given for (a) the induced flow in a quiescent fluid and *valid only for specific* **ratios** *of the rates of rotation of the cylinders*, and (b) the steady motion with the fluid qui-

escent at infinity when the two-roll mill revolves like *a planetary system* about a particular focus situated on their line of centers. To the authors knowledge, no new solutions have been published ever since analyzing the problem of Stokes flow for a corotating two-roll mill. Here, a general solution is presented for the Stokes flow induced by two cylinders of equal radii and corotating at the same angular speed in a quiescent fluid, and capable of fast, accurate predictions.

The lack of analytical solutions for some configuration of mills has not hampered the use of these devices for experimental studies. In particular, two- and four-roll mills have been frequently used in the laboratory to study the effects of two-dimensional elongational flow upon embedded objects. These flow geometries provide the means of generating a complete class of strong flows at the critical point located between the cylinders, with a variety of possible rates of deformation applicable to deformable bodies. Astarita [8], and Olbricht *et al.* [9] have classified two-dimensional steady flows as strong or weak flows. Strong flows are those that have locally a larger rate of deformation than its vorticity, with weak flows being those dominated by vorticity; simple shear flows correspond to the upper limit of weak flows and have a ratio of rate of deformation to vorticity equal to one. Hence strong flow can cause large deformations to an embedded deformable body in contrast with the small deformations achievable only with steady, weak flows. Furthermore, the residence time for an embedded object at the stagnation point can be extremely long, allowing studies of its dynamics under a large set of known conditions.

These latter characteristics make the two- and four-roll mills useful devices for many studies in low Reynolds number hydrodynamics. Indeed, these mills have been used to study the dynamics of drops, capsule, emulsions, etc., and more recently the dynamics of chaotic or mixing systems, with significant responses observed when using these strong flows as compared to simple shear or purely extensional flows. In 1932, G.I. Taylor [10, 11] performed some of the earliest experiments of a drop deformation due to a strong flow field generated by a four-roll mill. More recently, Leal and coworkers [12–15] have used a computer-controlled four-roll mill to study the dynamics of drops suspended in a viscous fluid. These studies have provided a clearer understanding of the effects of the viscosities of the fluids, surface tension, surfactant additives, etc. Rallison [16] and Stone [17] have recently summarized the theoretical, experimental and numerical studies of the dynamics of drops and bubbles in well-characterized flows with ratios of the rate of deformation to vorticity well in excess of the characteristic value for simple shear flow. Finally, Chang and Olbricht [18] have studied the dynamics of breakup of *elastic capsules* filled with a liquid under purely elongational and simple shear flow conditions. Ottino and coworkers [19] have recently studied Stokes flows generated by a *blinking* two-roll mill contained inside a third rotating cylinder. However and because of the intrinsic noise of numerical simulations, Ottino and collaborators [19] emphasize the need for analytical solutions of the flow field of complex Stokes flows: small changes in the numerical calculated velocity field can produce very different advection patterns. Finally, Leal and coworkers [20–22] have used a two- and four-roll mill configuration to study the flow field of non-Newtonian fluids subjected to elongational flows with vorticity. Among those studies, special emphasis has been given to studies of the dynamics of polymeric liquids [23] its optical properties and the evaluation of constitutive equations for fluids subjected to strong flows. Hence the spectrum of applications of the analytical solution of the Stokes flow of two-roll mills can provide useful insight for a large number of problems in fluid mechanics. Also these studies have relevance to a large number of industrial applications (*e.g.*, see Stone [17]).

Given the usefulness of two- and four-roll mills, for the study of a slow, strong flow, it is now important to emphasize the different options that these two systems offer to the experimentalist. For the four-roll mill, the rotational speed of the cylinders sets the shear rate, and the ratio of the speeds of next to each other rollers sets the ratio of vorticity to rate of deformation that exist at the stagnation point. However, in contrast with the two-roll mill, and on one hand, the four-roll mill requires an experimental determination of the proportionality constants that express the shear rate as a function of the speed of the cylinders. Furthermore, there is no analytical solution for the Stokes flow generated with a four-roll mill when the position and size of the cylinders needs to be taken into account. On the other hand, there is no need to vary the geometrical form of the device in order to vary the ratio of the rate of deformation to vorticity that exists at the stagnation point as needed with the two-roll mill set-up, a condition that has prompted an undue disregard for the two-roll mill hydrodynamics. This apparent drawback of the experimental studies reported until now is mainly due to the concomitant perturbations to the two-dimensionality of the flow as a result of presence of boundaries along the axes of rotation of the cylinders, which is dependent of the ratio of cylinders' length to the gap between them. These have been important limitations to experimental studies using strong flows with large vorticity such as those generated by a two-roll mill, because comparisons of experimental data against theoretical or numerical results are often difficult to correlate. However for many studies, the application of similar techniques to those used by Bentley and Leal [12] can reduce significantly the adverse effects of boundaries in two-roll mills. Finally, the four-roll mill only requires to change the relative speed of diagonally opposed rollers to modify the ratio of vorticity to rate of deformation. It generates a well defined flow when small vorticities are needed, but does not provide an adequate flow field when the ratio of speeds of next to each other cylinders is large; *i.e.*, when ratios of rate of deformation to vorticity have values close to one. Under these circumstances, the two-roll mill is a better device to generate 2-D strong flows.

The contents of this paper are as follows. In Sect. 2 the mathematical solution for the flow induced by a corotating two-roll mill is presented in cylindrical bipolar coordinates.

Jeffery's solution for the biharmonic equation together with the symmetry properties of the flow field are used to obtain the Fourier series expansion of the stream function. The series allows the calculation of the flow properties in closed-form to the required precision; the convergence of the truncated series is analyzed with respect to the accuracy of the prediction of flow parameters. Finally in Sect. 3, the flow field in the neighborhood of the stagnation point is studied, giving emphasis to the most relevant parameters for the study of embedded bodies. For the flow about the stagnation point, Stokes flow solution is compared with the solution of Dunlap [24] valid only locally. Furthermore, these analytical results are compared with numerical results [20] and experimental measurements of the principal components of the velocity gradient tensor [22].

2. The solution for creeping flows generated by two-roll mills

2.1. Geometry, and governing equations in cylindrical bipolar coordinates

The corotating two roll mill is best described using cylindrical bipolar coordinates. Figure 1 shows a two-roll mill with parallel cylinders of equal radii R, and separated by a gap g. In cylindrical bipolar coordinates a point on the plane $P(x, y)$ is represented by two vectors $\mathbf{r}_A$ and $\mathbf{r}_B$, plus two angles θ_A, and θ_B respectively, drawn from two fixed points A and B which are symmetrically located from the origin at a distance d. In this manner the bipolar coordinates (α, β, z') are

$$\alpha = \ln\left(\frac{\| \mathbf{r}_B \|}{\| \mathbf{r}_A \|}\right) \quad \text{and} \quad \beta = \theta_A - \theta_B,$$

with the 3-dimensional space (x, y, z) described by

$$\mathbf{P} = \frac{d\sin\beta}{\cosh\alpha - \cos\beta}\mathbf{i}_1 + \frac{d\sinh\alpha}{\cosh\alpha - \cos\beta}\mathbf{i}_2 + z\,\mathbf{i}_3, \quad (1)$$

where $\mathbf{P}$ is a point, and $\{\mathbf{i}_i\}$ is the Cartesian base. This is a *conjugate* cylindrical coordinate system, and hence it is an *orthogonal* curvilinear coordinate system perpendicular to the z-axis. The metric factor h can be expressed in terms of the metric coefficients $\mathbf{g}_k$

$$\mathbf{g}_1 = \frac{\partial \mathbf{P}}{\partial\alpha} = -\frac{d\sinh\alpha\sin\beta}{(\cosh\alpha - \cos\beta)^2}\mathbf{i}_1 + \frac{d(1 - \cosh\alpha\cos\beta)}{(\cosh\alpha - \cos\beta)^2}\mathbf{i}_2, \quad (2)$$

$$\mathbf{g}_2 = \frac{\partial \mathbf{P}}{\partial\beta} = \frac{d(\cosh\alpha\cos\beta - 1)}{(\cosh\alpha - \cos\beta)^2}\mathbf{i}_1 - \frac{d\sinh\alpha\sin\beta}{(\cosh\alpha - \cos\beta)^2}\mathbf{i}_2, \quad (3)$$

$$\mathbf{g}_3 = \frac{\partial \mathbf{P}}{\partial z'} = \mathbf{i}_3; \quad (4)$$

such that

$$\frac{\partial \mathbf{P}}{\partial q_k} = \frac{\partial x}{\partial q_k}\mathbf{i}_1 + \frac{\partial y}{\partial q_k}\mathbf{i}_2 + \frac{\partial z}{\partial q_k}\mathbf{i}_3, \quad (q_k = \alpha, \beta, \text{or } z'). \quad (5)$$
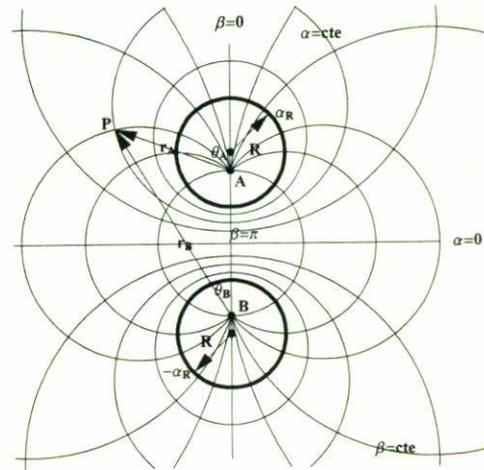

FIGURE 1. The configuration of the two-roll mill in cylindrical bipolar coordinates (α, β, z'). For $\alpha = $ constant, a family of eccentric circles above and below the x-axis is generated. For constant values of β a second family of circles is generated with centers on the x-axis. All circles ($\beta = $ constant) intersect at the point d along the y-axis, which also corresponds to the limit of circles when α tends to ∞. Two cylinders of radii R are shown as $\alpha = \alpha_R$. The center of the xy coordinate system corresponds to $(\alpha = 0, \beta = \pi)$.

And the metric tensor is

$$(g_{kl}) = \begin{pmatrix} \dfrac{d^2}{(\cosh\alpha - \cos\beta)^2} & 0 & 0 \\ 0 & \dfrac{d^2}{(\cosh\alpha - \cos\beta)^2} & 0 \\ 0 & 0 & 1 \end{pmatrix}$$

so that

$$g_{11} = g_{22} = h_{11}^2 = h_{22}^2 = h^2. \quad (6)$$

Furthermore, this coordinate system is characterized by the following relations

$$x^2 + y^2 - d^2 - 2dx\cot\beta = 0, \quad (7)$$

and

$$(y - d\coth\alpha)^2 + x^2 = d^2\text{csch}^2\alpha. \quad (8)$$

Hence, for $\beta = $ constant (with values between $0 \leq \beta \leq 2\pi$) a family of circles is generated with their centers located on the x-axis at $(d\cot\beta, 0)$, and with radii equal to $d\csc\alpha$. Each circle passes through the points A and B. For $\alpha = $ constant, a second set of circles is generated with their centers located on the y-axis at $(0, d\coth\alpha)$ and radii $d\,\text{csch}\,\alpha$. In this manner, at every point $\mathbf{P}(x, y)$ a circle of each family intersect *orthogonally*, allowing its representation with a unique set (α, β). The point A corresponds to $\alpha = +\infty$ and B to $\alpha = -\infty$. $\beta = 0$ corresponds to vertical lines above A and below B, and $\beta = \pi$ generates the segment (A, B). The origin corresponds to $\alpha = 0$ and $\beta = \pi$, and a point at infinity is defined by $\alpha, \beta = 0$. A more detailed description of the bipolar coordinate system is given in Appendix A of Ref. 4.

The two-roll mill is described by selecting constant values of $\alpha = \pm\,\alpha_R$, with α playing the role of the tangential coordinate, and β being the normal coordinate to the cylinders. The geometric aspects of the two-roll mill are defined by

$$\frac{g}{2R} = \cosh\alpha_R - 1, \quad \text{and} \quad d = R\sinh\alpha_R. \qquad (9)$$

Now, consider an isothermal, incompressible, Newtonian fluid, under laminar flow conditions generated by a two-roll mill. The fluid velocity $\mathbf{u}$ and the hydrodynamic pressure P are governed by the continuity and the Navier-Stokes equations

$$\nabla\cdot\mathbf{u} = 0, \qquad \frac{D\mathbf{u}}{Dt} = -\frac{1}{\rho}\nabla P + \nu\nabla^2\mathbf{u},$$

where ρ is the density, and ν is the kinematic viscosity of the fluid. Let l_c and U_c be the characteristic length and velocity of the flow such that a characteristic Reynolds number is $\mathrm{Re} = \rho l_c U_c/\mu$. Then, the *dimensionless* governing equations for a quasi-steady, creeping flow are

$$\nabla^2\mathbf{u} - \nabla p = 0, \qquad (10)$$

$$\nabla\cdot\mathbf{u} = 0. \qquad (11)$$

This equation is exactly valid for Reynolds number equal to zero, and is also a good approximation for small values of the Reynolds number. For a two-dimensional flow a simpler equation prescribes the creeping flow in terms of the stream function. That is, the velocity components u and v along the x and y directions can be expressed in terms of the stream function as

$$u = \frac{\partial\psi}{\partial y}, \quad v = -\frac{\partial\psi}{\partial x},$$

and the vorticity ω as

$$\omega = \frac{\partial v}{\partial x} - \frac{\partial u}{\partial y} = \nabla^2\psi.$$

With the above equations, the pressure can be eliminated from Eq. (10) and

$$\frac{1}{2}\mathrm{Re}\left(\frac{\partial\omega}{\partial t} + \frac{\partial\psi}{\partial y}\frac{\partial\omega}{\partial x} - \frac{\partial\psi}{\partial x}\frac{\partial\omega}{\partial y}\right) = \nabla^2\omega,$$

and the solution of the flow field must satisfy the biharmonic equation

$$\nabla^4\psi = 0. \qquad (12)$$

2.2. Jeffery's Stream Function of a two-roll mill in bipolar coordinates

In 1920, Jeffery [5] presented a solution for the biharmonic equation in bipolar coordinates used to study the stresses generated on a flat plate with round holes. In 1922, Jeffery used this solution to study the internal flow field generated by two eccentric circular cylinders. The stream function proposed is given as a Fourier series expansion

$$\frac{\psi}{h} = A_0\cosh\alpha + B_0\alpha\left(\cosh\alpha - \cos\beta\right) + C_0\sinh\alpha$$
$$+ D_0\alpha\sinh\alpha + K\left(\cosh\alpha - \cos\beta\right)\ln\left(\cosh\alpha - \cos\beta\right)$$
$$+ \left[A_1\cosh\left(2\alpha\right) + B_1 + C_1\sinh\left(2\alpha\right)\right]\cos\beta$$
$$+ \left[A_1'\cosh\left(2\alpha\right) + C_1'\sinh\left(2\alpha\right)\right]\sin\beta$$
$$+ \sum_{n=2}^{\infty}\left[\phi_n\left(\alpha\right)\cos\left(n\beta\right) + \phi_n'\left(\alpha\right)\sin\left(n\beta\right)\right], \quad (13)$$

where the metric factor

$$h = \frac{d}{\left(\cosh\alpha - \cos\beta\right)}, \qquad (14)$$

and the coefficient of the Fourier series are

$$\phi_n\left(\alpha\right) = A_n\cosh\left(n+1\right)\alpha + B_n\cosh\left(n-1\right)\alpha$$
$$+ C_n\sinh\left(n+1\right)\alpha + D_n\sinh\left(n-1\right)\alpha, \quad (15)$$

and

$$\phi_n'\left(\alpha\right) = A_n'\cosh\left(n+1\right)\alpha + B_n'\cosh\left(n-1\right)\alpha$$
$$+ C_n'\sinh\left(n+1\right)\alpha + D_n'\sinh\left(n-1\right)\alpha. \quad (16)$$

Given that the two-roll mill has equal cylinders rotating at equal speeds, the flow field must be anti-symmetric with respect to reflections upon the x- or y-axis as shown in Fig. 2. In order to take advantage of the simplification due to the symmetry properties, the velocity field in terms of the stream function is needed. Hence,

$$\mathbf{u} = \nabla\times\psi = \frac{1}{h^2}\begin{vmatrix} h\mathbf{e}_1 & h\mathbf{e}_2 & \mathbf{e}_3 \\ \dfrac{\partial}{\partial\alpha} & \dfrac{\partial}{\partial\beta} & \dfrac{\partial}{\partial z} \\ 0 & 0 & \psi \end{vmatrix} = \frac{1}{h}\frac{\partial\psi}{\partial\beta}\mathbf{e}_1 - \frac{1}{h}\frac{\partial\psi}{\partial\alpha}\mathbf{e}_2$$

The velocity component tangential to the surface of the cylinders is

$$u_\alpha = \frac{1}{h}\frac{\partial\psi}{\partial\beta} = \frac{\partial}{\partial\beta}\left(\frac{\psi}{h}\right) - \left(\frac{\psi}{h}\right)\frac{1}{h}\frac{\partial}{\partial\beta}\left(\frac{1}{h}\right); \quad (17)$$

that is,

$$u_\alpha = B_0\alpha\sin\beta + K[\ln(\cosh\alpha - \cos\beta) + 1]\sin\beta$$
$$- (A_1\cosh 2\alpha + B_1 + C_1\sinh 2\alpha)\sin\beta$$
$$+ (A_1'\cosh 2\alpha + C_1'\sinh 2\alpha)\cos\beta$$
$$+ \sum_{n=2}^{\infty}\{-n[A_n\cosh(n+1)\alpha + B_n\cosh(n-1)\alpha$$
$$+ C_n\sinh(n+1)\alpha + D_n\sinh(n-1)\alpha]\sin n\beta$$
$$+ n[A_n'\cosh(n+1)\alpha + B_n'\cosh(n-1)\alpha$$
$$+ C_n'\sinh(n+1)\alpha + D_n'\sinh(n-1)\alpha]\cos n\beta\}$$
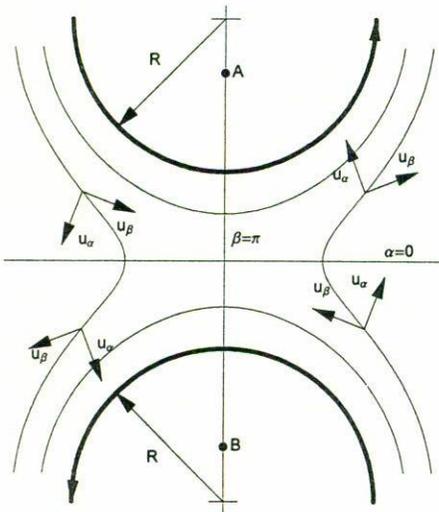$$- \frac{\psi}{h}\frac{\sin\beta}{\cosh\alpha - \cos\beta}. \qquad (18)$$

FIGURE 2. The velocity field and its velocity components $\mathbf{u}_\alpha$, and $\mathbf{u}_\beta$ in bipolar coordinates. The symmetry lines $\alpha = 0$, and $\beta = \pi$ are shown. The symmetry properties of the stream function are obtained using the symmetry properties of $\mathbf{u}_\alpha$, and $\mathbf{u}_\beta$ near the stagnation point where the components are parallel to the Cartesian coordinates.

The velocity component normal to the cylinders

$$u_\beta = -\frac{1}{h}\frac{\partial \psi}{\partial \alpha} = -\frac{\partial}{\partial \alpha}\left(\frac{\psi}{h}\right) + \left(\frac{\psi}{h}\right)\frac{1}{h}\frac{\partial}{\partial \alpha}\left(\frac{1}{h}\right), \quad (19)$$

and

$$u_\beta = -A_0 \sinh \alpha - B_0 \left[(\cosh \alpha - \cos \beta) + \alpha \sinh \alpha\right]$$

$$- C_0 \cosh \alpha - D_0 (\alpha \cosh \alpha + \sinh \alpha)$$

$$- K \sinh \alpha \left[1 + \ln (\cosh \alpha - \cos \beta)\right]$$

$$- (2A_1 \sinh 2\alpha + 2C_1 \cosh 2\alpha) \cos \beta$$

$$- (2A_1' \sinh 2\alpha + 2C_1' \cosh 2\alpha) \sin \beta$$

$$- \sum_{n=2}^{\infty} \{[A_n(n+1) \sinh (n+1)\alpha$$

$$+ B_n(n-1) \sinh(n-1)\alpha$$

$$+ C_n(n+1) \cosh(n+1)\alpha$$

$$+ D_n(n-1) \cosh (n-1)\alpha] \cos n\beta$$

$$+ [A_n'(n+1) \sinh (n+1)\alpha$$

$$+ B_n'(n-1) \sinh(n-1)\alpha$$

$$+ C_n'(n+1) \cosh (n+1)\alpha$$

$$+ D_n'(n-1) \cosh (n-1)\alpha] \sin n\beta\}$$

$$+ \frac{\psi}{h}\frac{\sinh \alpha}{\cosh \alpha - \cos \beta}. \quad (20)$$

In Fig. 2 the symmetry properties of the velocity field are shown; in particular for the components of the velocity field u_α, and u_β, which allow an initial reduction of the

coefficients that must be determined. That is, at the center $(\alpha = 0, \beta = \pi)$ there is a stagnation point. This "stagnation point" exists along an axis parallel to the cylinders axes, and therefore should be strictly referred to as the *stagnation line* of the flow field. For simplicity it is referred here as the stagnation point, although it may refer to a line running along the flow and perpendicular to the curvilinear coordinate system. On the xy-plane and above the stagnation point, for a counter-clockwise rotation of cylinders, material points move to the left, while below it, all material points move towards the opposite direction with the same speeds as the one located at the same distance above the center. This flow pattern implies that for those points near the horizontal line ($\alpha \simeq 0$) the velocity component u_α, when α tends to 0 from above, $u_\alpha(0^+)$, must have the same value and direction as when α tends to 0 from below $u_\alpha(0^-)$. Also, the velocity component u_β must have equal values but opposite sign when crossing the horizontal line. That is,

$$\forall \beta : \quad \left\{ \begin{array}{l} u_\alpha(\alpha \to 0^-) = u_\alpha(\alpha \to 0^+) \\ u_\beta(\alpha \to 0^-) = -u_\beta(\alpha \to 0^+) \end{array} \right\}.$$

A similar condition exists between the left and right side of the flow field: material points on the right side are displaced upwards on the right and downward on the left side. In the neighborhood around the line joining the centers of the cylinders (when $\beta \simeq \pi$), the velocity component u_α, when β tends to π from the right, $u_\alpha(\pi^+)$, must have the same value and but opposite direction as when β tends to π from the left $u_\alpha(\pi^-)$. Also, the velocity component parallel to the x-axis, u_β, must have the same value when β tends to π from the right and left. Hence,

$$\forall \alpha : \quad \left\{ \begin{array}{l} u_\alpha(\beta \to \pi^-) = -u_\alpha(\beta \to \pi^+) \\ u_\beta(\beta \to \pi^-) = u_\beta(\beta \to \pi^+) \end{array} \right\}.$$

Imposing these symmetry conditions upon the velocities implies that the coefficients $B_0, C_0, C_1, C_n, C_n', D_n$, and D_n' must all be equal to zero. Then, the stream function reduces to

$$\frac{\psi}{h} = A_0 \cosh \alpha + D_0 \alpha \sinh \alpha$$

$$+ K (\cosh \alpha - \cos \beta) \ln (\cosh \alpha - \cos \beta)$$

$$+ \sum_{n=1}^{\infty} [A_n \cosh(n+1)\alpha + B_n \cosh(n-1)\alpha] \cos n\beta. \quad (21)$$

Using Eq. (A.7), the logarithmic term can be expressed as a cosine series and the stream function is

$$\frac{\psi}{h} = A_0 \cosh \alpha + D_0 \alpha \sinh \alpha$$

$$+ K \left(b_0 + b_1 \cos \beta + \sum_{n=2}^{\infty} b_n \cos n\beta\right)$$

$$+ \sum_{n=1}^{\infty} [A_n \cosh(n+1)\alpha + B_n \cosh(n-1)\alpha] \cos n\beta, \quad (22)$$

with coefficients $b_0 + b_1$ and b_n given by Eqs. (A.8).

2.3. Boundary conditions satisfied by the stream function

On the cylinder's walls, the boundary condition prescribing the impenetrability of the surface implies that the velocity component normal to the roller is zero; that is

$$u_\alpha\left(\alpha_R\right) = \left|\frac{1}{h}\frac{\partial\psi}{\partial\beta}\right|_{\alpha_R} = 0, \qquad (23)$$

where α_R is the cylinder radius given in bipolar coordinates. The dynamic no-slip boundary condition is

$$u_\beta\left(\alpha_R\right) = -\left|\frac{1}{h}\frac{\partial\psi}{\partial\alpha}\right|_{\alpha_R} = \omega R, \qquad (24)$$

with ω being the angular velocity in radians, and R is the cylinder radius. At infinity, the fluid must remain at rest and

$$\psi\left(\alpha\to 0, \beta\to 0\right) = 0 \qquad (25)$$

for the velocity to be $\mathbf{u}\left(\alpha\to 0, \beta\to 0\right) = \mathbf{0}$. That is, the stream function valued far from the cylinders implies that

$$A_0 + \sum_{n=1}^{\infty}\left(A_n + B_n\right) = 0. \qquad (26)$$

The condition of no-flow through the cylinder's walls is set by a constant value for the stream function, say M, so that

$$\begin{aligned}
\frac{1}{h}\psi\left(\alpha_R, \beta\right) &= \left(\frac{\cosh\alpha - \cos\beta}{d}\right)M \\
&= A_0\cosh\alpha_R \\
&\quad + K\left[b_0 + b_1\cos\beta + \sum_{n=2}^{\infty}b_n\cos n\beta\right] \\
&\quad + D_0\alpha_R\sinh\alpha_R \\
&\quad + \sum_{n=1}^{\infty}[A_n\cosh(n+1)\alpha_R \\
&\qquad\qquad +B_n\cosh(n-1)\alpha_R]\cos n\beta \qquad (27)
\end{aligned}$$

Collecting those terms of same $\cos n\beta$ order the first system of $n+2$ equations is obtained

$$\left(A_0 - \frac{M}{d}\right)\cosh\alpha_R + D_0\,\alpha_R\sinh\alpha_R + K\,b_0 = 0, \qquad (28)$$

$$\frac{M}{d} + A_1\cosh 2\alpha_R + B_1 + Kb_1 = 0, \qquad (29)$$

and for $n \geq 2$,

$$A_n\cosh(n+1)\alpha_R + B_n\cosh(n-1)\alpha_R + Kb_n = 0. \qquad (30)$$

The no-slip boundary condition on the cylinders surface, $u_\beta\left(\alpha_R\right) = \omega R$, implies

$$\begin{aligned}
\omega R = &-A_0\sinh\alpha_R \\
&- D_0\left(\alpha_R\cosh\alpha_R + \sinh\alpha_R\right) + \frac{M}{d}\sinh\alpha_R \\
&- K\sinh\alpha_R\left(1 + a_0 + \sum_{n=1}^{\infty}a_n\cos n\beta\right) \\
&- \sum_{n=1}^{\infty}[A_n(n+1)\sinh(n+1)\alpha_R \\
&\qquad\qquad +B_n(n-1)\sinh(n-1)\alpha_R]\cos n\beta. \qquad (31)
\end{aligned}$$

And collecting terms of equal $\cos n\beta$ order, a second system of $n+2$ equations is obtained,

$$\begin{aligned}
A_0\sinh\alpha_R + &D_0\left(\alpha_R\cosh\alpha_R + \sinh\alpha_R\right) \\
&+ K\sinh\alpha_R\left(1 + a_0\right) - \frac{M}{d}\sinh\alpha_R + \omega R = 0, \qquad (32)
\end{aligned}$$

$$2A_1\sinh 2\alpha_R + Ka_1\sinh\alpha_R = 0, \qquad (33)$$

and for $n \geq 2$,

$$\begin{aligned}
A_n(n+1)&\sinh(n+1)\alpha_R \\
&+ B_n(n-1)\sinh(n-1)\alpha_R + Ka_n\sinh\alpha_R = 0. \qquad (34)
\end{aligned}$$

There are $2n+4$ unknowns: A_0, A_1, A_n, B_1, B_n, D_0, K and M; but only $2n+3$ equations. Given that M corresponds to the value of the stream function ψ on the surface of the cylinders, set arbitrarily by the computation, any constant value can be used. Therefore, the solution consists of a system of $2n+3$ equations and unknowns. Equations (30) and (34) imply that

$$\frac{A_n}{K} = \frac{(n+1) - e^{-2n\alpha_R} - ne^{-2\alpha_R}}{n(n+1)\left[n\sinh 2\alpha_R + \sinh 2n\alpha_R\right]}, \qquad (35a)$$

$$\frac{B_n}{K} = \frac{(n-1) + e^{-2n\alpha_R} - ne^{2\alpha_R}}{n(n-1)\left[n\sinh 2\alpha_R + \sinh 2n\alpha_R\right]}. \qquad (35b)$$

The remaining coefficients are

$$A_0 = \frac{2R\omega\alpha_R\sinh\alpha_R - 2K\left[b_0\left(\sinh\alpha_R + \alpha_R\cosh\alpha_R\right) - \left(1 + a_0\right)\alpha_R\sinh^2\alpha_R\right]}{2\alpha_R + \sinh 2\alpha_R}, \qquad (36a)$$

$$A_1 = -\frac{Ka_1\operatorname{sech}\alpha_R}{4}, \qquad (36b)$$

$$B_1 = -Kb_1 + \frac{Ka_1\coth 2\alpha_R\sinh\alpha_R}{2}, \qquad (36c)$$

$$D_0 = -\frac{A_0\cosh\alpha_R + Kb_0}{\alpha_R\sinh\alpha_R}. \qquad (36d)$$

The last coefficient K can be expressed using Eqs. (27), (36), and (37) as follows:

$$A_0 = -\sum_{n=1}^{\infty}(A_n + B_n) = -A_1 - B_1 - \sum_{n=2}^{\infty} K\left(\frac{A_n}{K} + \frac{B_n}{K}\right) \quad (37)$$

and

$$A_0 + A_1 + B_1 = -K \sum_{n=2}^{\infty} \left(\frac{A_n}{K} + \frac{B_n}{K}\right) \equiv -KS, \quad (38)$$

where

$$S = \sum_{n=2}^{\infty} \frac{(-2n)e^{-2n\alpha_R} + (n-n^2)e^{-2\alpha_R} + (n+n^2)e^{2\alpha_R}}{n(n-1)(n+1)(n\sinh 2\alpha_R + \sinh 2n\alpha_R)}. \quad (39)$$

Consequently,

$$K = -4R\omega\alpha_R \sinh\alpha_R \Big[2S(2\alpha_R + \sinh 2\alpha_R)$$

$$+ 4\alpha_R(a_0 + 1)\sinh^2\alpha_R - 4b_0(\sinh\alpha_R + \alpha_R\cosh\alpha_R)$$

$$- 2b_1(2\alpha_R + \sinh 2\alpha_R)$$

$$+ a_1\Big(2\alpha_R\coth 2\alpha_R \sinh\alpha_R - \alpha_R\mathrm{sech}\alpha_R$$

$$- \frac{3}{2}\sinh\alpha_R + \frac{1}{2}\sinh 3\alpha_R\Big)\Big]^{-1}. \quad (40)$$

Finally, the explicit form of the stream function for Stokes flow generated by the two-roll mill is given by Eqs. (23), (35), (36), and (40). Figure 3 shows the stream functions for two different geometries of the two-roll mill. The geometrical parameters for these mills corresponds to those given by Geffroy and Leal [25] where the distance between the cylinder axes is maintained fixed and the cylinder's radii changes. That is, the value for the parameter d takes a different value for every pair of rollers.

3. The Stokes flow about the stagnation point

The kinematic conditions at the stagnation point located between the cylinders is perhaps the region of the flow field most frequently used until now for studies of the dynamics of non-Newtonian fluids. For example, Dunlap [24] studied the dynamics of various dilute polymeric solutions under the flow conditions that exist in the neighborhood of the stagnation point assuming kinematics similar to those prevalent for Newtonian fluids. In particular, the correlation of polymer deformations induced by the flow and the rates of deformation applied by the flow is a critical parameter for those experiments. More recently, Wang et al. [22] have studied the flow field of polymeric liquids using the homodyne light scattering technique [26] (a method capable of measuring directly the most relevant flow parameters) in order to determine the flow conditions that affect the deformation of the polymeric structure. One of the most relevant aspect of these studies is the fact that the *flow-type parameter* and the *shear rate* of the flow at the stagnation point have been directly related to the rate of rotation of the rollers and the geometry of the two-roll mill.
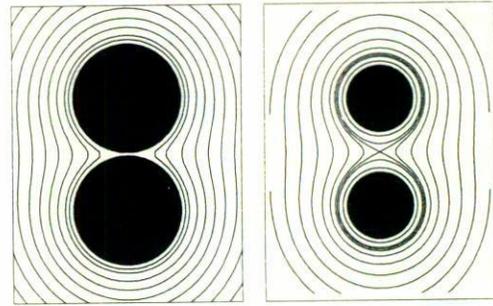

FIGURE 3. The streamlines for two different geometries of the two-roll mill. The distance from the center to the axes of the cylinders is 0.017 m for both devices. The cylinder's radii are 0.01665 m and 0.01075 m, for the left and right configuration respectively, which corresponds to rollers A and I of Table I.

3.1. Shear rate and value of the flow-type parameter at the stagnation point

With the equation for the stream function it is possible to obtain a simpler expression, valid in the neighborhood of the stagnation point, by using a Taylor series expansion about $\alpha = 0$ and $\beta = \pi$ and keeping only terms up to second order. That is, $y \cong d\alpha/2$ and $x \cong d(\pi - \beta)/2$, and Eq. (23) becomes

$$\left[\frac{2 - 2x^2 + 2y^2}{d}\right]\psi = A_0(1 + 2y^2) + 4y^2 D_0$$

$$+ K\left[4y^2\left(\frac{1 - x^2 - \ln 2}{8}\right) + 2\ln 2 - 2x^2(1 + \ln 2)\right]$$

$$+ \sum_{n=1}^{\infty}(-1)^n(1 - 2n^2x^2)\Big\{A_n[1 + 2y^2(n+1)^2]$$

$$+ B_n[1 + 2y^2(n-1)^2]\Big\}. \quad (41)$$

In this equality, the left term is proportional to $(1 - x^2 + y^2)$. Multiplying both sides by $(1 + x^2 - y^2)$, then the left side is $(1 - x^2 + y^2)(1 + x^2 - y^2) = 1 - x^4 + 2x^2y^2 - y^4 \approx 1$, valid up to quartic order. Therefore, Eq. (41) becomes

$$\frac{2}{d}(1 - x^2 + y^2)(1 + x^2 - y^2)\psi \approx \frac{2\psi}{d}$$

$$\approx A_0 + 2K\ln 2 + \sum_{n=1}^{\infty} i^{2n}(A_n + B_n)$$

$$+ y^2\Big(A_0 + 4D_0 + 2K$$

$$+ \sum_{n=1}^{\infty} i^{2n}\big\{2[A_n(n+1)^2 + B_n(n-1)^2] - [A_n + B_n]\big\}\Big)$$

$$+ x^2\Big\{A_0 - 2K + \sum_{n=1}^{\infty} i^{2n}[(A_n + B_n) - 2n^2(A_n + B_n)]\Big\}.$$

The stagnation point is characterized by a saddle point, which implies that the coefficients for the x^2 and y^2 have opposite signs. In this manner, the stream function can then be expressed as a 2-dimensional hyperbolic flow $y^2 - \lambda x^2 = c$,

with

$$\lambda = -\frac{A_0 - 2K + \sum_{n=1}^{\infty} i^{2n}[(A_n + B_n) - 2n^2(A_n + B_n)]}{A_0 + 4D_0 + 2K + \sum_{n=1}^{\infty} i^{2n}\{2[A_n(n+1)^2 + B_n(n-1)^2] - (A_n + B_n)\}}, \tag{42}$$

and

$$c = \frac{(2/d)\psi - A_0 - 2K\ln 2 - \sum_{n=1}^{\infty} i^{2n}(A_n + B_n)}{A_0 + 4D_0 + 2K + \sum_{n=1}^{\infty} i^{2n}\{2[A_n(n+1)^2 + B_n(n-1)^2] - (A_n + B_n)\}}. \tag{43}$$

Furthermore, given the linear character of Stokes equations, the velocity field at the stagnation point can be expressed by

$$\mathbf{u} \cong \nabla \mathbf{u}^T \cdot \mathbf{x}, \tag{44}$$

where

$$\begin{bmatrix} u_x \\ u_y \end{bmatrix} \cong \dot{\gamma} \begin{bmatrix} 0 & 1 \\ \lambda & 0 \end{bmatrix} \begin{bmatrix} x \\ y \end{bmatrix},$$

and

$$\nabla \mathbf{u}\Big|_{(\alpha=0,\beta=\pi)} = \begin{bmatrix} 0 & \dfrac{2}{d}\dfrac{\partial u_\alpha}{\partial \beta} \\ \dfrac{2}{d}\dfrac{\partial u_\beta}{\partial \alpha} & 0 \end{bmatrix}.$$

The expansion for u_α and u_β as a Taylor series up to quadratic terms and about $(\alpha = 0, \beta = \pi)$ is

$$u_\alpha = \frac{x}{d}\left\{ -A_0 + 2K + \sum_{n=1}^{\infty} i^{2n}[(2n^2 - 1)(A_n + B_n)] \right\},$$

and

$$u_\beta = \frac{-y}{d}\left(A_0 + 4D_0 + 2K \right.$$
$$\left. + \sum_{n=1}^{\infty} i^{2n}\left\{ 2\left[A_n(n+1)^2 + B_n(n-1)^2 \right] - (A_n + B_n) \right\} \right).$$

Since both the Cartesian and bipolar coordinate systems are orthogonal, then at the stagnation point $\mathbf{x}'$,

$$u_y \cong u_\alpha(\mathbf{x}'), \text{ and } u_x \cong -u_\beta(\mathbf{x}').$$

Therefore, based upon Eq. (44) the velocity components can be recast as

$$\begin{bmatrix} u_x \\ u_y \end{bmatrix} = \begin{bmatrix} \dot{\gamma} y \\ \dot{\gamma} \lambda x \end{bmatrix},$$

where $\dot{\gamma}$ is the *magnitude of the velocity gradient or the shear rate* of the flow at the stagnation point and is given by

$$\dot{\gamma} = \frac{1}{d}\left(A_0 + 4D_0 + 2K + \sum_{n=1}^{\infty} i^{2n}\left\{ 2\left[A_n(n+1)^2 \right. \right. \right.$$
$$\left. \left. \left. + B_n(n-1)^2 \right] - (A_n + B_n) \right\} \right), \tag{45}$$

and the *flow-type parameter* or *degree of extensional flow*, λ, is given by Eq. (42). For the two-roll mill geometry, the flow-type attains values larger than zero (but smaller than one); a value of zero corresponds to the case of simple shear flow and
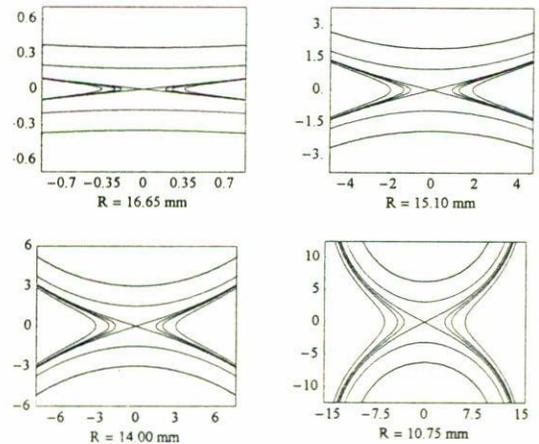

FIGURE 4. Streamlines in the vicinity of the stagnation point for different geometries of the two-roll mill. (a) $R = 16.65$ mm; (b) $R = 15.10$ mm; (c) $R = 14.00$ mm; (d) $R = 10.75$ mm. The angle sustained by the asymptotic streamlines at the stagnation point corresponds to 2θ, and are the most probable orientation for a highly deformed body embedded in the flow.

can only be reached when the gap between the cylinders is infinitesimally small, *i.e.*, $\alpha_R \to 0$. Figure 4 presents the streamlines in the vicinity of the stagnation point for two different geometries.

When analyzing the dynamics of polymeric liquids, changes of the fluid microstructure are easily measured by evaluating the flow-induced optical anisotropy. In these studies, the orientation of the polymer anisotropy occurs near the outgoing axes of the hyperbolic flow. The angle sustained by the asymptotic lines of the hyperbolic flow (when $c \to 0$) is defined by

$$2\theta_f = \arctan\left(\frac{y}{x}\right) = \arctan\left(\lambda^{\frac{1}{2}}\right), \tag{46}$$

with θ_f being the angle of an asymptote and the x-axis. θ_f corresponds to the orientation of the principal eigenvector of the velocity gradient tensor $\nabla \mathbf{u}$, and also corresponds to the most probable orientation of an immersed, deformed body, since the principal eigenvector of the rate of deformation tensor $\mathbf{D} = (\nabla\mathbf{u} + \nabla\mathbf{u}^T)$ is also aligned at this angle. Even for the simplified solution about the stagnation point, the orientation angle and the flow-type parameter depend only upon the geometrical characteristics of the two-roll mill. For a slightly

deformed body or a fluid with microstructure, the alignment with respect to the flow must have an angle $\theta_f \leq \theta \leq \pi/4$. The upper limit corresponds to a two-dimensional *pure extensional* flow, and for flows close to simple shear the lowest value is near zero. The experimentally observed values for θ, smaller than θ_f, as reported for polymeric liquids are the result of a strong modification of the local kinematics of the flow field due to the nonlinear effects introduced by non-Newtonian constitutive equations (see, for example, Ref. 25).

Dunlap [24] obtained an expression for the stream function valid at the stagnation point:

$$\psi = \frac{d^2 \omega}{\cosh \alpha - \cos \beta} \left(A_0 \cosh \alpha + D_0 \sinh \alpha \right), \qquad (47)$$

where

$$A_0 = \frac{\alpha_R}{\alpha_R + \sinh \alpha_R \cosh \alpha_R},$$

$$D_0 = -\frac{\coth \alpha_R}{\alpha_R + \sinh \alpha_R \cosh \alpha_R}. \qquad (48)$$

The flow-type parameter and the shear rate are, respectively,

$$\lambda = \left(\frac{4 \coth \alpha_R}{\alpha_R} - 1 \right)^{-1}, \qquad (49)$$

and

$$\dot{\gamma} = \frac{A_0 \omega}{\lambda}. \qquad (50)$$

This solution has several disadvantages, but as will be shown subsequently, this simplified solution is remarkably accurate about the stagnation point, and in particular for flow-type values close to those of simple shear flow. Among its drawbacks are that it does not represent correctly the flow field far from the stagnation point, and it does not have the centers for the vorticity located at the axes of the cylinders. Instead they coincide with points A and B; that is, for $\alpha \to \infty$. As a result, the extent of the region about the stagnation point with kinematic conditions determined by the above values of $\dot{\gamma}$, λ, and θ is unknown in relation to the length-scales defined by the geometry of the mill.

3.2. Flow parameters for experimental two-roll mill configurations

Two-roll mill flow devices have been used in the past, especially to study the dynamics of polymeric fluids (see, for example, Refs. 20, 22, 24, and 25). The advantage of the use of the two-roll mill for these studies is the fact that the flow-type parameter is larger than zero, but corresponds to a extensional flow field with significant amounts of vorticity, in particular when the values achieved are compared to values accessible with a four-roll mill configuration. That is, when the conformation of the fluid structure can be altered significantly by the degree of extensional flow, then the use of two-roll mill is superior since the response of the fluid can be more easily differentiated due to the presence of vorticity causing a less drastic deformation of the microstructure.

TABLE I. Dimensions for the two-roll mill with different sizes of diameters for the cylinders. For all cases, the distance between rollers's axes is fixed at 17.0 mm. d corresponds to the distance from the center of the flow cell (the stagnation point) to the position along the y-axis where $\alpha \to \infty$ and allows the representation of the rollers by α_R

Roller	Radii (mm)	gap (mm)	d (mm)
A	16.65	0.70	3.431836
B	16.35	1.30	4.655910
C	15.70	2.60	6.519969
D	15.10	3.80	7.809609
E	14.17	5.66	9.392076
F	14.00	6.00	9.643651
G	12.78	8.44	11.210334
H	11.69	10.62	12.342767
I	10.75	12.50	13.169567

3.2.1. Geometrical parameters

In studies reported by Geffroy and Leal [25], the two-roll mill geometry is such that the centers of the cylinders is maintained fixed at 0.0170 m, while eight different sets of rollers is used to vary the flow parameters. Table I lists the diameters of the cylinders and the gap existing between them. The calculated value for half the distance between points A and B (d), and which allows the representation of the cylinders' surface by a constant value of $\alpha = \alpha_R$, is also given and is always larger that the separation between cylinders.

3.2.2. The flow type parameter

Given the geometric characteristics of the flow devices it is now possible to compare the precision of the calculated values of the flow parameters. Table II presents the values of the flow-type parameter using the approximated expression (λ_{approx}) by Dunlap [24], Stokes solution [given by Eqs. (23), (35), (36), and (40)], the numerical value reported by Singh and Leal [20], and the experimental values by Wang *et al.* [22]. This Table considers three possible precisions for the summations implied by Eq. (39) and obtained by truncating the sum after $n = 5$, 25, and 125 terms. The entries without values in the numerical and experimental columns imply that these are not available.

It is clear that the flow-type values predicted for the complete range of flow devices is approximately the same when more than 25 terms of the summation are considered. In fact, the latter criteria is adequate for λ values greater than 0.04. The number of terms required at low values of λ increases and, surprisingly, provides values equivalent to those obtained with the simplified expression of Dunlap. Figure 5 presents the dependence of the calculated value of the flow-type parameter on the number of terms of the sum [Eq. (39)]. The plot corresponds to the two-roll mill configuration with

TABLE II. Calculated values of the flow type, λ, as a function of the flow device geometry and evaluated at the stagnation point. $\lambda_{\mathrm{approx}}$ corresponds to the predicted values using Dunlap's expression, and λ_n are those evaluated using Eq. (42) with n the number of summands considered. λ_{num} and λ_{exp} are the numerical and experimental results reported in Refs. 20, and 22, respectively.

| Roller	$\lambda_{\mathrm{Approx}}$	$\lambda\,(n=5)$	$\lambda\,(n=25)$	$\lambda\,(n=125)$	λ_{num}	λ_{exp}
A	0.0104379	0.115312	0.0105409	0.0104379	...	...
B	0.0196209	0.0988742	0.0196247	0.0196209	...	...
C	0.0403169	0.0810291	0.040316	0.040316	...	0.047
D	0.060474	0.081976	0.060461	0.060461	...	0.067
E	0.093974	0.102122	0.094123	0.094123	...	0.096
F	0.100424	0.107371	0.100692	0.100692	...	0.114
G	0.150133	0.154612	0.152789	0.152789	0.153	0.160
H	0.200548	0.207745	0.207191	0.207191	...	0.196
I	0.297712	0.259299	0.259108	0.259108	...	...
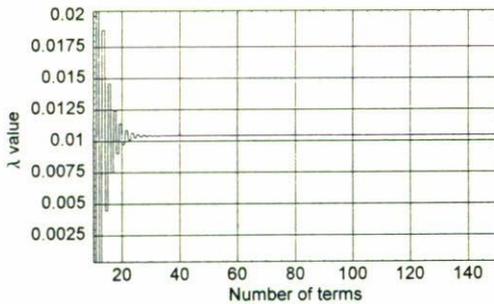
FIGURE 5. Convergence of calculated values for the flow-type parameter, λ, as a function of the number of terms before truncation of the analytic solution for the stream function.

the smallest gap (rollers A) since its computation presents the weakest convergence behavior. For this mill, whenever more that 40 terms in the summation are taken into account the value for λ hardly changes. For the results given here, the sums are truncated after 125 terms.

3.2.3. The magnitude of the velocity gradient tensor

The magnitude of the velocity gradient at the stagnation point is another important parameter for these flows. That is, given a fixed maximum angular velocity of rotation of the cylinders provided by a set of motors, the top shear rate that the mill can produce is a function of its geometry via the tangential speed and the gap between rollers. For the same two-roll mill geometries, Table III presents the values of the normalized shear rates (with respect to the angular speed of the cylinders) as calculated by the expression of Dunlap ($\dot{\gamma}_D/\omega$), the exact solution (considering 125 terms), and the experimental values obtained by Wang *et al.* ($[\dot{\gamma}/\omega]_{\mathrm{exp}}$). However, in this table, the second and fourth left most columns are found using the full solutions as given by Eqs. (47) and (48) for Dunlap's expression, and Stokes solution based on Eqs. (23), (35), (36), and (40). The first and third columns are obtained using the expressions valid about the stagnation point.

TABLE III. Magnitude of the principal eigenvalue of the velocity gradient tensor, normalized with respect to the angular speed of the cylinders. $[\dot{\gamma}_D/\omega]_{\mathrm{approx}}$ and $[\dot{\gamma}_D/\omega]$ are the predicted values based upon Dunlap's expression. $[\dot{\gamma}/\omega]_{\mathrm{approx}}$ and $[\dot{\gamma}/\omega]$ are the predicted values for the locally and globally valid Stokes solution, respectively. $[\dot{\gamma}/\omega]_{\mathrm{exp}}$ are the reported results of Wang *et al.* [22].

Roller	$\left[\dfrac{\dot{\gamma}_D}{\omega}\right]_{\mathrm{approx}}$	$\dfrac{\dot{\gamma}_D}{\omega}$	$\left[\dfrac{\dot{\gamma}}{\omega}\right]_{\mathrm{approx}}$	$\dfrac{\dot{\gamma}}{\omega}$	$\left[\dfrac{\dot{\gamma}}{\omega}\right]_{\mathrm{exp}}$
A	47.237331	47.239904	47.237331	47.239904	...
B	24.819154	24.823931	24.819154	24.823931	24.1
C	11.741155	11.750694	11.741156	11.750694	11.7
D	7.610899	7.624803	7.610783	7.624681	7.84
E	4.670160	4.690736	4.669733	4.690372	4.83
F	4.329777	4.351555	4.329427	4.351319	4.44
G	2.692708	2.722886	2.695945	2.727231	2.80
H	1.868669	1.905877	1.87967	1.919587	1.84
I	1.391422	1.434168	1.41084	1.457431	...

Figure 6 presents a comparison of λ values calculated with the exact solution and Dunlap's expression. It is clear that for large gaps (small cylinders radii), the expression valid at the stagnation point overestimates the values of the flow-type parameter; in fact, λ can have unrealistic values larger than one. The series solution attains the expected limiting values of $\lambda = 0$ for the smallest gap, and $\lambda = 1$ when the rollers have a minimum diameter. As shown in Table II, both the approximate expression and the complete solution have discrepancies of less than one percent for $\lambda < 0.2$. For values $0.2 < \lambda < 0.4$, the calculated values differ, but the two-roll mill geometry has not been used for such large values although it appears to be a useful geometry for λ values as high as 0.8. However, for such large values, the four-roll mill may be a better alternative to generate elongational flows
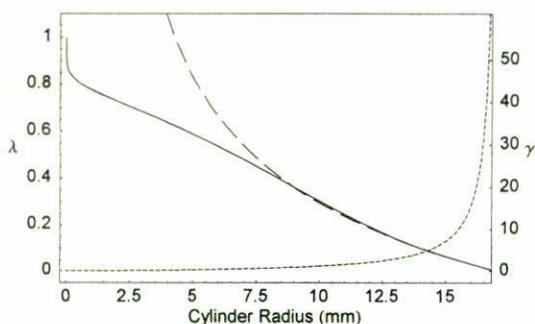
FIGURE 6. Calculated values for the flow-type parameter using the approximate expression of Dunlap [24] (the dotted line) and the series expansion given here (continuous line) with truncation after 125 terms. The separation between cylinders' axes is 0.034 m. Dunlap's expression predicts unrealistic values whenever the radii of the cylinders are less than 0.0043 m. The series solution predicts the correct values for the largest ($\lambda = 0$) and smallest radii ($\lambda = 1$).

with small amounts of vorticity since according to Table III it is obvious that the magnitude of the accessible shear rates can be extremely limited for two-roll mills with a large-λ-value configuration. The available range of shear rates with a four-roll mill is not as severely limited as is the case of the two-roll mill.

4. Discussion and conclusions

A solution valid for zero Reynolds number flows generated by two-roll mills is given. This solution can be a useful benchmark for a number of elongational creeping flows because its flow parameters evaluated at the stagnation point can be accurately known. Also, this solution could be useful as a first order approximation for studies of inertial effects (nonzero Reynolds numbers) or non-Newtonian constitutive equations, and to perform stability analyses of the full 3D-flow field. Inertial effects may disrupt the symmetric properties of the flow field; in particular, the streamlines for fluid parcels approaching the stagnation point will tend to curve faster, while those departing from the stagnation point will follow patterns close to the central line (x-axis). Furthermore, this solution could be useful to study a new class of nonsteady flows, or the Stokes paradox present far from the stagnation point [4]. When studying non-Newtonian constitutive equations, this flow field may present smaller values for the shear rates and flow type as a result of nonzero normal stresses. In the case of hydrodynamic instabilities, the two-dimensional character of the zero Reynolds number flow field could be modified.

Even for nonzero Reynolds numbers, the present solution can be useful as a benchmark for a number of experimental and numerical techniques used to study the flow field near the central stagnation point. As shown in Tables II and III, The available experimental values are slightly higher that the numerical and theoretical predictions for the flow-type as

well as the shear rate, which may be a consequence of the fact that different models for the flow field were used. That is, the numerical simulation of Singh and Leal, and the experimental results of Wang et al., have used a two-roll mill contained inside a third circular cylinder with flat ends that conform the flow cell while the analytical results assumes an unbounded fluid domain. Furthermore, the third cylinder is stationary which represents a significant departure from the kinematic conditions implied by the unbounded domain. Consequently, for the numerical and experimental data, the presence of boundaries on the $\alpha\beta$-plane at a finite distance may affect the observed values for the flow parameters. However, for the flow field near the stagnation point the discrepancy with the theoretical calculations appear clearly at odds with the experimental values and less with the numerical result. This is true for the calculated values for the flow-type and the shear rate as shown in Tables II and III, especially for the set of rollers from C to G. It is not clear why this is the case, but perhaps these theoretical and numerical results can provide some insight into the accuracy of the experimental technique or as a benchmark to "fine-tune" the precision of the experimental measurements.

The significant drop of the measured value for λ and $\dot{\gamma}$ for the largest set of rollers H may be a consequence of significant three-dimensionality effects present for that configuration. That is, for these devices, the rollers are about 0.0254 m long and the length-to-gap ratio is only about two to one. The flow cell encloses the cylinders with non-slip boundary conditions at the extreme of the cylinders, and perpendicular to the axes. The flow field on the layers next the flat covers must be similar to that of simple shear flow, which implies that the observed value of λ may be dependent upon the depth of the flow cell. Furthermore, the velocity field may also be weaker due to the proximity of the container walls and the shear rate is consequently smaller. Hence, boundary effects normal to the rollers axes and due to the existence of flat surfaces may reduced the net value of the flow-type parameter especially when the gap is relatively large and even when it is evaluated at the central position of the "stagnation line" as shown in Table II; these conditions can also reduced the measured shear rate as given in Table III. If this assertion is correct, then two-roll mill flow cells need to consider a design with a significantly larger value for the length to gap ratio for all rollers, or the means to reduced the friction at the walls, in order to determine a consistent flow-type parameter for geometries with large values of λ.

Acknowledgments

Appendix A

The solution of the stream function valid for the two-roll mill requires an equivalent expression for the logarithmic term that appears in Eq. (21). A simple Fourier series solution can be found when the following relation is used [27]:

$$\ln\left(1 - 2x\cos\phi + x^2\right) = -2\sum_{n=1}^{\infty}\frac{\cos n\phi}{n}x^n. \quad (A.1)$$

Since

$$\ln\left(x + \sqrt{1 + x^2}\right) = \sinh^{-1}x;$$

$$x^2 \leq 1 \quad \text{and} \quad x\cos\phi \neq 1,$$

Equation (52) can be cast as

$$\ln\left(\frac{1 + x^2}{2x} - \cos\phi\right) = -\ln(2x) - 2\sum_{n=1}^{\infty}\frac{\cos n\phi}{n}x^n.$$

From the above equation, the logarithmic term can be easily obtained with the change of variables $\phi = \beta$, and $\left(1 + x^2\right)/2x = \cosh\alpha = \varrho$, such that the following equality:

$$1 - 2x\varrho + x^2 = 0,$$

has solutions

$$x = \frac{-(-2\varrho) \pm \sqrt{4\varrho^2 - 4}}{2} = \varrho \pm \sqrt{\varrho^2 - 1}$$

$$= \cosh\alpha \pm \sqrt{\cosh^2\alpha - 1} = \cosh\alpha \pm \sinh\alpha$$

$$= \frac{(e^\alpha + e^{-\alpha}) \pm (e^\alpha - e^{-\alpha})}{2} = \frac{(1 \pm 1)e^\alpha + (1 \mp 1)e^{-\alpha}}{2}.$$

Hence,

$$x = e^{\pm\alpha}.$$

This last equation must have only one solution. For $\alpha > 0$, and $x^2 \leq 1$, only the negative root is valid. Therefore, applying the change of variables on the tabulated equality [Eq. (A.1)] with the relation for x imply that

$$\ln(\cosh\alpha - \cos\beta) = -\ln\left(2e^{-\alpha}\right) - 2\sum_{n=1}^{\infty}\frac{\cos n\beta}{n}e^{-n\alpha}$$

$$= \alpha - \ln 2 - 2\sum_{n=1}^{\infty}\frac{e^{-n\alpha}}{n}\cos n\beta$$

$$= a_0 + \sum_{n=1}^{\infty}a_n\cos n\beta, \quad (A.2)$$

where

$$a_0 = \alpha - \ln 2 \quad \text{and} \quad a_n = -2\frac{e^{-n\alpha}}{n}. \quad (A.3)$$

The left side of expression for the stream function is multiplied by the $(\cosh\alpha - \cos\beta)$ term. Hence, from Eqs. (A.2)

and (A.3) the right most term is the logarithmic summand is

$$\cos\beta\ln\left(\cosh\alpha - \cos\beta\right) = \left(a_0 + \sum_{n=1}^{\infty}a_n\cos n\beta\right)\cos\beta$$

$$= a_0\cos\beta + \sum_{n=1}^{\infty}a_n\cos\beta\cos n\beta.$$

Using the identity $\cos\beta\cos n\beta = \frac{1}{2}\cos(n+1)\beta + \frac{1}{2}\cos(n-1)\beta$, the sum of the latter equation can be written as

$$\sum_{n=1}^{\infty}a_n\cos\beta\cos n\beta =$$

$$\sum_{n=1}^{\infty}\frac{a_n}{2}\left[\cos(n+1)\beta + \cos(n-1)\beta\right]$$

$$= \frac{a_1}{2}\cos 2\beta + \frac{a_1}{2} + \frac{a_2}{2}\cos 3\beta + \frac{a_2}{2}\cos\beta$$

$$+ \sum_{n=3}^{\infty}\frac{a_n}{2}\left[\cos(n+1)\beta + \cos(n-1)\beta\right],$$

and with some further simplifications

$$\sum_{n=1}^{\infty}a_n\cos\beta\cos n\beta = \frac{a_1}{2} + \frac{a_2}{2}\cos\beta$$

$$+ \sum_{n=2}^{\infty}\left(\frac{a_{n+1}}{2} + \frac{a_{n-1}}{2}\right)\cos n\beta. \quad (A.4)$$

In this manner,

$$\cos\beta\ln(\cosh\alpha - \cos\beta) = \frac{a_1}{2} + \left(a_0 + \frac{a_2}{2}\right)\cos\beta$$

$$+ \sum_{n=2}^{\infty}\left(\frac{a_{n+1}}{2} + \frac{a_{n-1}}{2}\right)\cos n\beta. \quad (A.5)$$

The remaining term becomes

$$\cosh\alpha\ln(\cosh\alpha - \cos\beta) =$$

$$a_0\cosh\alpha + \sum_{n=1}^{\infty}a_n\cosh\alpha\cos n\beta$$

$$= a_0\cosh\alpha + a_1\cosh\alpha\cos\beta$$

$$+ \sum_{n=2}^{\infty}a_n\cosh\alpha\cos n\beta; \quad (A.6)$$

Hence, the product $(\cosh\alpha - \cos\beta)\ln(\cosh\alpha - \cos\beta)$ can be obtained from Eqs. (A.5) and (A.6) so that

$$(\cosh\alpha - \cos\beta)\ln(\cosh\alpha - \cos\beta) =$$

$$\cosh\alpha\ln(\cosh\alpha - \cos\beta) - \cos\beta\ln(\cosh\alpha - \cos\beta)$$

$$= a_0\cosh\alpha + a_1\cosh\alpha\cos\beta + \sum_{n=2}^{\infty}a_n\cosh\alpha\cos n\beta$$

$$- \frac{a_1}{2} - \left(a_0 + \frac{a_2}{2}\right)\cos\beta - \sum_{n=2}^{\infty}\left(\frac{a_{n+1}}{2} + \frac{a_{n-1}}{2}\right)\cos n\beta,$$

or equivalently,

$$(\cosh\alpha - \cos\beta)\ln(\cosh\alpha - \cos\beta) = \left(a_0\cosh\alpha - \frac{a_1}{2}\right) + \left(a_1\cosh\alpha - a_0 - \frac{a_2}{2}\right)\cos\beta$$

$$+ \sum_{n=2}^{\infty}\left(a_n\cosh\alpha - \frac{a_{n+1}}{2} - \frac{a_{n-1}}{2}\right)\cos n\beta.$$

Finally,

$$(\cosh\alpha - \cos\beta)\ln(\cosh\alpha - \cos\beta) = b_0 + b_1\cos\beta + \sum_{n=2}^{\infty}b_n\cos n\beta, \qquad (A.7)$$

with

$$b_0 = a_0\cosh\alpha - \frac{a_1}{2}, \qquad (A.8a)$$

$$b_1 = b_1\cosh\alpha - a_0 - \frac{a_2}{2}, \qquad (A.8b)$$

$$b_n = a_n\cosh\alpha - \frac{a_{n+1}}{2} - \frac{a_{n-1}}{2}. \qquad (A.8c)$$

1. M.S. Chong, A.E. Perry, and B.J. Cantwell, *Physics Fluids A* **2** (1990) 765.

2. G.B. Jeffery, *Roy. Soc. Proc. A* **101** 169 (1922).

3. Sir H. Lamb, *Hydrodynamics*, 6th edition, (Cambridge UP, Cambridge, England, 1932) p. 68.

4. J. Happel and H. Brenner, *Low Reynolds number hydrodynamics*, (Kluwer Acad. Publ., Dordrecht, The Netherlands, 1991) p. 497.

5. G.B. Jeffery, *Philos. Trans. A* **221** (1920) 265.

6. R.A. Frazer, *Philos. Trans. A* **225** (1925) 93.

7. Sir G.G. Stokes, *Mathematical and physical papers*, (Cambridge UP, Cambridge, England, 1883).

8. G. Astarita, *J. Non-Newtonian Fluid Mech* **6** (1979) 69.

9. W.L. Olbricht, J.M. Rallison, and L.G. Leal, *J. Non-Newtonian Fluid Mech.* **10** (1982) 291.

10. G.I. Taylor, *Proc. R. Soc. London Ser. A* **138** (1932) 41.

11. G.I. Taylor, *Proc. R. Soc. London Ser. A* **146** (1934) 501.

12. B.J. Bentley and L.G. Leal, *J. Fluid Mech.* **167** (1986) 219.

13. B.J. Bentley and L.G. Leal, *J. Fluid Mech.* **167** (1986) 241.

14. H.A. Stone, B.J. Bentley, and L.G. Leal, *J. Fluid Mech.* **173** (1986) 131.

15. W.J. Milliken, H.A. Stone, and L.G. Leal, *Phys. Fluids A* **5** (1993) 69.

16. J.M. Rallison, *Ann. Rev. Fluid Mech.* **16** (1984) 45.

17. H.A. Stone, *Ann. Rev. Fluid Mech.* **26** (1994) 65.

18. K.S. Chang and W.L. Olbricht, *J. Fluid Mech.* **250** (1993) 609.

19. S.C. Jana, G. Metcalfe, and J.M. Ottino, *J. Fluid Mech.* **269** (1994) 199.

20. P. Singh and L.G. Leal, *J. Non-Newtonian Fluid Mech.* **67** (1996) 137.

21. J. Feng and L.G. Leal, *J. Non-Newtonian Fluid Mech.* **72** (1997) 187.

22. J.J. Wang, D. Yavich, and L.G. Leal, *Phys. Fluids* **6** (1994) 3519.

23. D. Yavich and L.G. Leal, *Rheol. Acta* **34** (1995) 360.

24. P.N. Dunlap, Ph. D. Thesis, California Institute of Technology, (1986).

25. E. Geffroy and L.G. Leal, *J. Polym. Sci.; Polym. Phys.* **30** (1992) 1329.

26. G.G. Fuller, J.M. Rallison, R.L. Schmidt, and L.G. Leal, *J. Fluid Mech.* **100** (1980) 555.

27. I.S. Gradshteyn and I.M. Ryzhik, *Table of integrals, Series and Products. Corrected and Enlarged Edition*, (Academic Press, San Diego, USA, 1981) Eq. 1.514.